Screening and rooting the multiple anomalies of Nepal earthquake sequence in 2015 with DTS criterion and homologous LCAI-coupling physics

Lixin Wu[1, 2], Yuan Qi[1, 2], Wenfei Mao[1, 2], Jingchen Lu[1, 2], Yifan Ding[1, 2], Boqi Peng[1, 2] and Busheng Xie[1, 2]

[1] School of Geosciences and Info-Physics, Central South University, Changsha, 410083, China

5   [2] Laboratory of Geo-Hazards Perception, Cognition and Predication, Central South University, Changsha, China

Correspondence to: Wenfei Mao (maowenfei@csu.edu.cn)

Abstract. The continuously increasing of earth observations benefits geosciences and seismicity study, but increases greatly the difficulties in understanding and discriminating multiple source data. Although the Lithosphere-Coversphere-Atmosphere-Ionosphere (LCAI) coupling paradigm and the Deviation-Time-Space (DTS) criterion were presented for better searching for

10   and understanding the potential seismic anomalies from multiple observations, the strict consistency of spatio-temporal characteristics and homologous physics of multiple-parameter seismic anomalies has not been investigated sufficiently. With the 2015 Nepal earthquake sequence being a typical case, the reported multi-parameter anomalies were systematically reviewed, and their space-time characteristics were summarized thoroughly in this study. Numerical simulation with refined geological structures in three-dimensional space revealed the inhomogeneous crustal stress field alternation (CSFA) along the

15   faults and around the hypocentres of 2015 Nepal earthquake sequence, which is expected to be the root of the seismic anomalies. The stress-activated positive charge carriers would have given rise to different responses near the ground surface (coversphere), including the microwave dielectric reduction, the additional infrared radiation, and the atmospheric ionization, which subsequently affected the physical properties of atmosphere and ionosphere and resulted in abnormal phenomena therein. Based on the DTS criterion and LCAI coupling paradigm, the seismic anomalies of 2015 Nepal earthquakes were screened

20   strictly, and the screened-out anomalies were rooted carefully to the regional CSFA as well as its local blocking. Therefore, an integrated LCAI coupling framework with strict space-time correspondence and homologous physics in CSFA was proposed for the 2015 Nepal earthquake sequence. This research provides a definite philosophy as well as a practical solution for screening out the rootable seismic anomalies from multi-parameter observations of earthquake, which is of scientific meanings for searching earthquake precursor and reaching earthquake prediction.

25   **1 Introduction**

Earthquake is one of the major natural disasters impacting greatly on human life and social development. The geophysical processes of the gestation and occurrence of earthquake is very complicated, which is always accompanied by mass migration, energy release and information exchange (Teng 2001). Supported with increasing earth observations, studies on earthquake

perception, cognition and prediction have achieved a lot during the past decades. The information acquisition of
30 seismic/tectonic activity has developed from the ground stations with limited number, uneven distribution and discontinuous
observation to the satellite platform with wide coverage, all-day and all-weather capability (Shen 2007; Shen et al., 2016; Jing
et al., 2008). The continuous enrichment of satellite missions and enhancement of observation capability have given rise to the
huge increment of data and information of seismicity, and provided great possibility for searching seismic anomalies and
earthquake precursors with collaborative analysis. However, the multiple-source observations on the information from beneath
35 the earth's surface, ground surface, atmosphere and ionosphere, and occur before, during and after the earthquake, have become
extremely complex, which make it tricky for researchers to judge the reliability of a single anomaly and to interpret the coupling
mechanism of multiple anomalies.

Although the crustal stress field alteration (CSFA) is commonly considered as the intrinsic cause of seismic anomalies, there
are many different opinions on how the atmosphere and ionosphere respond to CSFA. Great attempts have been devoted to
40 search for earthquake precursors and to explore its mechanisms (Gokhberg et al., 1985; Liperovsky et al., 1992; Liperovskaya
et al., 1994; Shalimov and Gokhberg, 1998; Sorokin and Chmyrev, 1998; Pulinets et al., 1994, 2000). Currently, the chain of
seismic anomalies observed in multiple spheres has been frequently reported (Pulinets and Ouzounov 2011; Wu et al., 2012a,
2016; Jing et al., 2019; Marchetti et al., 2020; Hayakawa et al., 2021; Qin et al., 2021; Jing and Singh, 2022). Two fundamental
hypothesis or theories, being mostly recognized, were presented to interpret the phenomena of chain-like seismic anomalies
45 appeared in multiple geospheres including lithosphere, coversphere, atmosphere and ionosphere. One is the radon emission-
and-decay, presented by Eurasian scientists such as Sergey Alexander Pulinets from Russia, who believes that tectonic activity
would release radon gas trapped originally in the soil and crust rock, and the air ionization due to radon decay will give rise to
multiple seismic anomalies; hence the other abnormal perturbances in aerosol, atmospheric humidity, latent heat, ionospheric
plasma and etc. were considered to be physically homologous with radon emission-and-decay (Pulinets and Boyarchuk 2004;
50 Pulinets 2009). The other is the activation-and-aggregation of positive holes (P-holes in brief), presented by American
scientists with Friedemann Freund being the important initiator (Freund et al., 2002, 2009, 2011), who believes that the
transition of P-holes from hypocentre and its accumulation on ground surface will change the earth's electromagnetic field and
ionize the air molecules at the ground-air interface, which subsequently give rise to a variety of abnormal phenomena in the
atmosphere and ionosphere (Freund et al., 2006, 2007, 2009; Kuo et al., 2011). The P-hole theory was initiated from rock
55 loading experiments, which discovered that the dormant peroxy bond could be activated by deviatoric rock stress and acts as
P-holes being able to transit from stressed rock to unstressed surface (Freund et al., 2002, 2006).

To explain synergically the seismic anomalies appeared in atmosphere and ionosphere above the seismogenious area, the
lithosphere-atmosphere-ionosphere (LAI) coupling paradigm was firstly presented to interpret the correlations of multiple
seismic anomalies and searching for potential mechanism of earthquake precursor (Liperovsky et al., 2008; Pulinets and
60 Ouzounov 2011). Considering that the geo-part between the lithosphere and atmosphere (soil, desert, water, ice and snow,
vegetation, etc.), called coversphere, has a vital impact on satellite observations and on the upward propagation of signals from
lithosphere in process of earthquake preparation, a lithosphere-coversphere-atmosphere (LCA) coupling paradigm was later

presented (Wu et al., 2012a, 2012b, 2016). Subsequently, the lithosphere-coversphere-atmosphere-ionosphere (LCAI) coupling paradigm, being the unity of LAI and LCA, has been presented and become a basic and integrated paradigm for

65   multi-parameter analysis of seismic anomalies (Zheng et al., 2014; Jing et al., 2019; Qin et al., 2021; Xiong et al., 2021). Meanwhile, inspired by the international consensus on the characteristics of seismic anomalies (Tronin 2000; Dey and Singh 2003; Genzano et al., 2009; Qin et al., 2012), a Deviation-Time-Space (DTS) criterion was proposed (Wu et al., 2012a; Qin et al., 2013) to investigate the correlations and reliability of abnormal variation of multiple parameters. The DTS criterion contains three parts: deviation of the parameter was notable enough to act as a potential anomaly; the occurrences of multiple

70   anomalies behave common features of quasi-synchronism in time and geo-adjacency in space.

Nevertheless, sometime we are not able to identify correctly the anomalies that seem to be related to an earthquake but have primal contradictions, such as contradictory effects or incorrect order of occurrence. A large earthquake usually causes numerous anomalies, which are assigned to different parameters and located in different spheres of the Earth. It is very challenging to screen out reliable anomalies from multiple parameters and explore their physical mechanisms. The joint

75   employment of DTS criterion and LCAI coupling paradigm is expected to be well in screening potential seismic anomalies with strict spatio-temporal consistency, and in rooting the seismic anomalies to CSFA with the same physical connotation, respectively.

The Mw 7.8 Gorkha earthquake in 2015 was the largest earthquake to strike the Himalayan arc in the past 70 years, and the strongest aftershock recorded a magnitude of Mw 7.3. The earthquake sequence attracted wide attention and a large number

80   of publications, which provides us a good case of studying how to screen reliable seismic anomalies from diversified reports. In this study, we reviewed carefully the reported multiple seismic anomalies associated with the 2015 Nepal earthquakes, and conducted a three-dimensional (3D) numerical simulation on the seismogenious process along the Himalayan. The root of the seismic anomalies was proved to be regional CSFA and local stress blocking. The reviewed seismic anomalies with physics homologous to the CSFA were strictly screened and rooted to a special LCAI coupling chain, which shared the homologous

85   physics as regional CSFA and behaved reasonable spatio-temporal pattern.

2 Case and methodology

2.1 Nepal earthquake sequence and geology background

The 2015 Nepal earthquake sequence began with a destructive Mw 7.8 earthquake 80 km northwest of Kathmandu (depth=8.2 km) on April 25, followed by a series of great aftershocks (see Fig. 1), including a great Mw 7.3 aftershock in Dolakha

90   (depth=15 km) on May 12. The earthquake sequence occurred in the front of the India-Eurasia collision belt, where is an extremely active area of geo-mechanical energy accumulation-and-release, many strong and devasting earthquakes had occurred along the belt in history (Kumar et al., 2006; Shan et al., 2015). The Gorkha earthquake and Dolakha aftershock were believed to be caused by a sudden release of built-up crustal stress along the major faults (Avouac et al., 2015). The Mw 7.8

mainshock and the Mw 7.3 aftershock generated a 60-km-wide×150-km-long rupture along the Main Himalayan Thrust (MHT)

95   fault, with an average slip of 3.5m and a local maximum slip being 7m at about 15 km north of Kathmandu (Mencin et al., 2015).

The Himalayan suture zone consists of several thrust faults (as in Fig. 1), including the Himalayan Main Frontal Thrust fault (MFT), the Main Boundary Thrust fault (MBT', differentiated from the abbreviation of microwave brightness temperature, MBT), the Main Central Thrust fault (MCT) and the detachment fault system in southern Tibet (Guo et al., 2009). The first

100   three faults expose on the ground surface and merge into the Main Himalayan Thrust fault (MHT) in the deep crust, the rupture of which was related to almost all the major earthquakes occurring on the Himalayan front fault (Bilham 2004). The Himalayan seismic belt also has obvious segmental activity characteristics. The eastern segment is accompanied by extrusion and clockwise rotation, the middle segment is dominated by extrusion, while the western segment is accompanied by counter-clockwise rotation (Su et al., 2015). The Nepal earthquake sequence in 2015 mainly occurred at the transferring zone of the

105   counter-clockwise rotation segment and clockwise rotation segment.
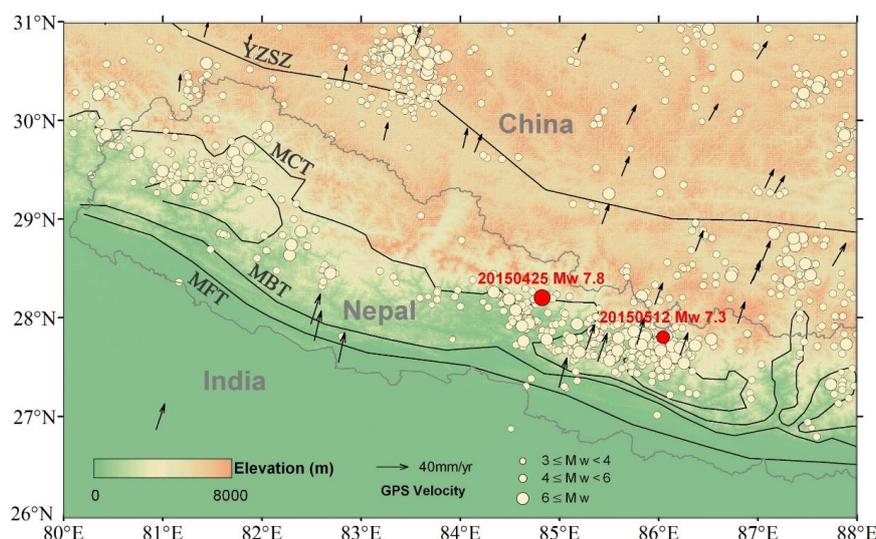
Figure 1: The distribution of earthquakes with magnitude greater than 3.0 in and nearby Nepal from 1912 to 2022. GPS velocity field refers to Su et al. (2015). Black arrows indicate the average velocities and directions of ground movement in 1990-2015 from GNSS observations (Kreemer et al., 2014; Zheng et al., 2017).

110   **2.2 Materials and methods**

In general, the LCAI coupling analysis of a seismic event requires lots of observations of multiple parameters. There are various methods for data processing and different knowledge backgrounds for studying the diversified parameters. Since the 2015 Gorkha earthquake and Dolakha earthquake occurred years ago, many researchers with knowledge of remote sensing, seismology, geophysics, respectively, have reported a large number of abnormal phenomena considered as seismicity-related,

115   which can be acquired from literatures so that the duplicated work on searching seismic anomalies can be avoided. A
preliminary screening of these literatures was firstly carried out, the basic criteria was referred to He et al. (2019), among
which the most critical factors to be considered were the clear space-time information and the specific physical connotation.
A total of more than 40 related literatures were then sorted out, including 22 abnormal parameters as in Tab. 1.

Table 1: Anomalous parameters in multiple geospheres reported on the 2015 Nepal earthquake sequence

Sphere	Parameter	Sphere	Parameter
Lithosphere	Deformation		Surface air temperature (SAT)
	Geo-electric filed		CO, NO$_2$, Ozone (O$_3$)
	Underground fluid		Air humidity
		Atmosphere	Aerosol optical depth (AOD)
Coversphere	Surface soil moisture (SSM)		Atmospheric chemical potential (ACP)
	Thermal infrared radiation (TIR)		Surface latent heat flux (SLHF)
	Snow surface temperature (SST)		Outgoing longwave radiation (OLR)
	Snow cover level		
	Land surface temperature (LST)		Geomagnetism
	Microwave brightness temperature (MBT)	Ionosphere	Vertical total electron content (TEC/VTEC)
	Soil radon (Rn)		Very/extremely low frequency (VLF/ELF)

120   Although the general spatio-temporal features of multiple-parameter anomalies can be obtained after the preliminary screening,
their spatio-temporal correlation and homologous physics still need to be strictly screened and rooted. Only those reported
anomalies behaving spatio-temporal consistency and sharing the homologous physics in CSFA can be regarded as reliable
seismic anomalies with potential earthquake precursor meanings. Eventually, an integrated LCAI coupling framework with
definite space-time-physics connotation will be retained after the strictly screening and physical rooting actions. The basic
125   flow diagram of this study is shown in Fig. 2.
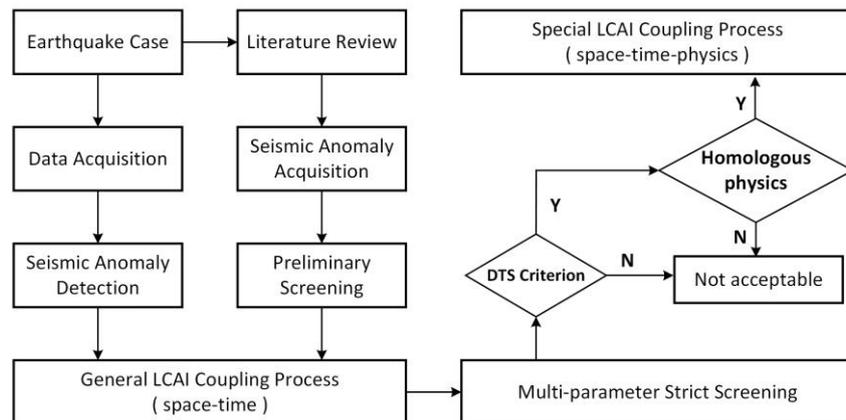
Figure 2: The technical route of screening and rooting multiple seismic anomalies using DTS criterion and homologous physics

3 Spatio-temporal features of reported seismic anomalies

3.1 Brief description of individual anomaly

130   For systematic summarization and clear comparison, the temporal characteristics and spatial distributions of all the reported seismic anomalies related to the Nepal earthquake sequence in 2015 are described in Fig. 3 and Fig.4, respectively, in a classification of lithosphere, coversphere, atmosphere and ionosphere.

In the lithosphere (Fig. 3 and 4b), the GPS velocity field shows that the continuous extrusion deformation between the Indian plate and the Eurasian plate had been significantly enhanced since 2012 (Zhan et al., 2015), which reflected that the

135   strengthened pushing effect of the Indian plate on the Qinghai-Tibet Plateau preceding the Gorkha earthquake. Coseismic displacement of the Gorkha earthquake and early postseismic (4-88 days after the mainshock) surface displacements were both detected by GPS and InSAR measurements (Shan et al., 2015; Sreejith et al., 2016). Observations of geoelectric field in Lhasa station (29.1º N, 91.0º E) showed that geoelectric anomaly had gradually appeared since June 2014 with the maximum variation exceeding 1000 mV/km. The geoelectric field tended to be stable 20d about before the mainshock with the variations remaining

140   below 100 mV/km, and showed very small disturbances after the Dolakha earthquake (Xi et al., 2016). The temperature of underground water at Yushu seismic station (33.0º N, 97.0º E) showed that water temperature had broken the normal upward trend since early March 2015, with a change rate of 48 times that of the original, and reached the peak one month about before the Gorkha earthquake (Yang et al., 2016). Besides, co-seismic underground water-level oscillation before and during the 2015 Nepal earthquakes were recorded in the Jingle well in Shanxi Province, China (38.4º N, 112.0º E) (He et al., 2017) and another

145   159 wells throughout the Chinese mainland. (Ma and Huang 2017).

In the coversphere (Fig. 3 and Fig. 4b), SSM around the epicenter areas behaved abnormally 10 and 5 days before the Gorkha earthquake, which had been excluded from the contribution of rainfall (Jing et al., 2019). Significant TIR anomalies were found to concentrated mainly to the west of the epicenter before the Gorkha earthquake by processing FY-2 satellite data (Lu et al. 2016; Zhang et al. 2017). TIR anomalies revealed by Zhang et al. (2017) started from middle March 2015, gradually

150   strengthened until the mainshock and then weakened afterwards. Lu et al. (2016) reported that TIR anomalies appeared in early April, peaked a week before the mainshock, then began to weaken and dissipate after the mainshock. Bhardwaj et al. (2017) found obvious departures in snow temperature 12d before and in snow cover level 20d before the Gorkha earthquake, by using of 16 years MODIS data. Chen et al. (2020) reported that a strip of LST appearing to the north of the epicenters along the Himalayas cooled slowly before, reached a minimum during and returned to normal after the Gorkha earthquake. Baral et

155   al. (2016) found distinct LST anomalies appeared 150 km about to the southwest of the epicenter on 18 April, which extended along the Main Himalayan Frontal Thrust (MFT) until 23 April, and dissipated one day before the Gorkha earthquake. LST was also found to exceed significantly the normal range around the epicenter 10d before the Gorkha earthquake (Shah et al. 2016). Jing et al. (2019) reported that significant MBT anomalies appeared to the west of the epicenter 10d before the mainshock. Positive MBT anomalies, reported by Qi et al. (2021), appeared shortly before, peaked on, and dissipated after the

160 occurrence of the two major earthquakes, respectively, with the abnormal stripes distributing along the Himalayas, covering the epicenters of the forthcoming earthquakes. The four-month simultaneous observations at two adjacent soil radon sites in Kolkata, India (22.6º N, 88.4º E) displayed two potential radon anomalies on April 20 and April 29 (Deb et al. 2016). Observations in Ghuttu, India (30.5º N, 78.8º E) also showed obvious variation of soil radon concentration in early April 2015, and a sudden increase from 10d before to 3d after the Gorkha earthquake (Kumar et al. 2017).
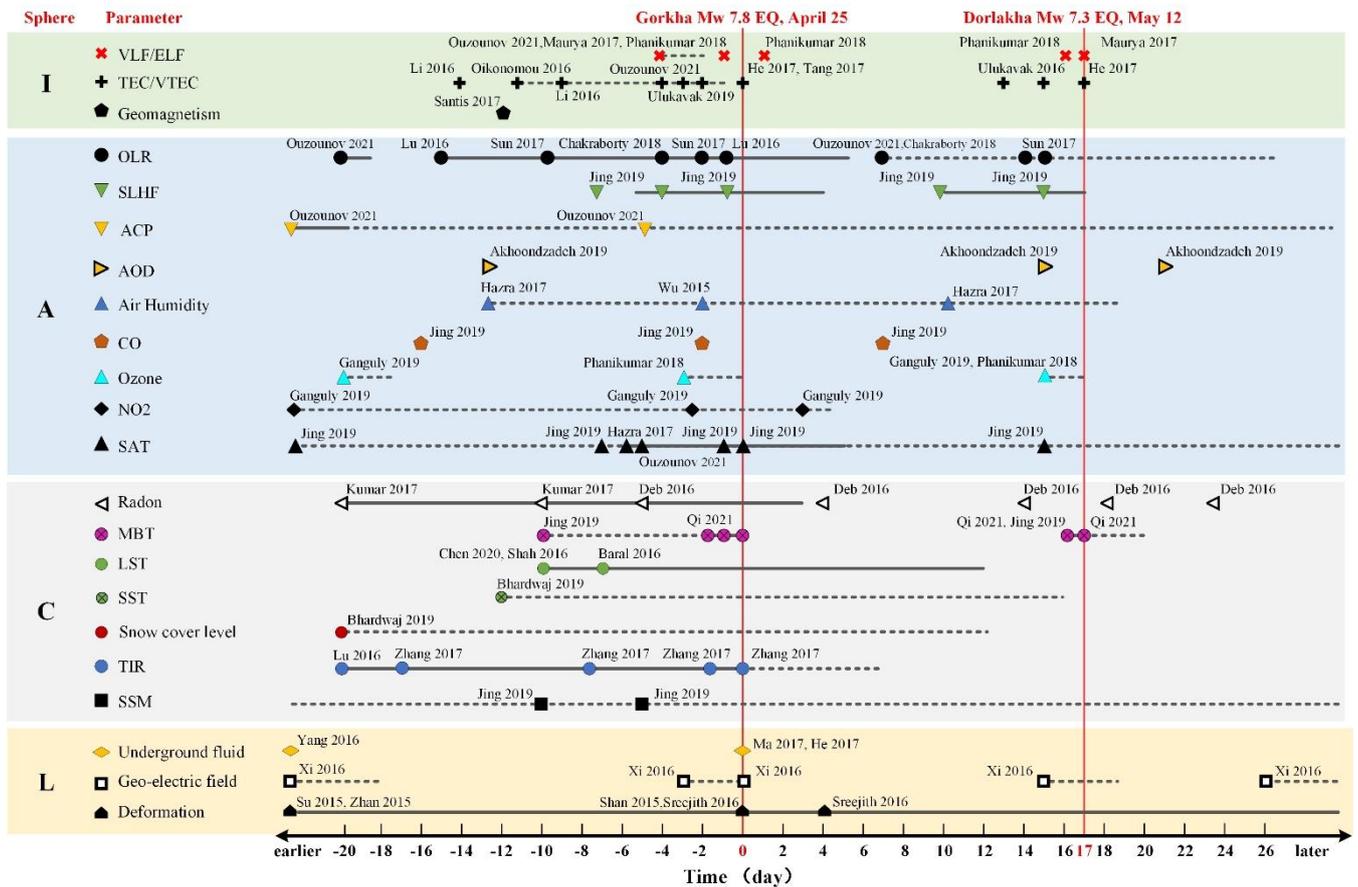
165

Figure 3: The temporal distribution of multiple anomalies from lithosphere up to ionosphere before, during and after the Gorkha earthquake and Dolakha earthquake in 2015. The dotted icon indicates that the anomaly occurred on a particular day, solid line means the anomaly was persistent, while dashed line means that the anomaly was fluctuant or intermittent.

170 In the atmosphere (Fig. 3 and 4c), Jing et al. (2019) reported that SAT from AIRS satellite over the epicentral and surrounding regions had behaved abnormally since 50d before the mainshock. Afterwards, the SAT anomaly peaked on the dates 7d and 1d before the Gorkha earthquake, and 2d prior to the Dolakha earthquake, respectively. Using NOAA Surface Data, Ouzounov et al. (2021) revealed that SAT anomalies appeared near the epicenters and peaked on the dates 5d before the Gorkha

earthquake and 7d prior to the Dolakha earthquake, respectively. Using SAT data from three stations near the mainshock epicenter, Hazra et al. (2017) found obvious SAT anomalies occurring 5-7 days before the Gorkha earthquake, which lasted for >10d. SLHF anomalies peaked on the date 1d prior to the Gorkha earthquake and disappeared 4d after, and then peaked on the date 3d prior to the Dolakha earthquake and dissipated afterwards (Jing et al. 2019). Using FY-2E satellite data, Lu et al. (2016) uncovered that OLR anomalies started from April 10, peaked on April 24 and then weakened, with anomalous region being strip-shaped cross the Nepal. By analysing NOAA time series, Chakraborty et al. (2018) found that OLR anomaly appearing around the epicenter started 3d prior to the mainshock and disappeared gradually after the earthquake, while Ouzounov et al. (2021) found that the OLR anomaly peaked around April 4-7 and May 2-3, 2015. Investigating the OLR data observed by FY-2D and NOAA, Sun et al. (2017) found that OLR anomaly occurred to the west of the future mainshock epicenters on April 15, peaked on April 24, dissipated subsequently, and reappeared 2d before the Dolakha earthquake.

Inside the atmosphere, tropospheric columnar NO_2 around the epicenter started increasing from 45d before and peaked on the date 3d after the Gorkha earthquake, and then oscillated in the next few months (Ganguly 2016). Two enhancements of columnar O_3 were observed in the same place 20d about before the Gorkha earthquake and 2d before the Dolakha earthquake, respectively, and then the amplitude of O_3 anomaly showed a downward trend (Ganguly 2016). In April 23-25 and May 10-12, 2015, the vertical profiles of mesospheric O_3 around the two epicenters had exceeded the normal threshold (Phanikumar et al. 2018). CO concentration (900 hPa) exhibited two abnormal enhancements in the southern region near the epicenters, 16d and 2d before the Gorkha earthquake and 10d before the Dolakha earthquake, respectively (Jing et al. 2019). Average atmospheric relative humidity from three meteorological stations near the mainshock epicenter reached minimal values 13d before the Gorkha earthquake and 7d before the Dolakha earthquake, respectively (Hazra et al. 2017). Wu et al. (2015) also reported a significant reduction in relative humidity at Kathmandu weather station 2d before the mainshock. Akhoondzadeh and Chehrebargh (2016) analysed the AOD data derived from MODIS and found that significant AOD anomaly at 550 nm appeared 13d and 2d prior to the Gorkha earthquake and Dolakha earthquake, respectively. Ouzounov et al. (2021) analysed the ACP data from the GEOS-5 assimilation and suggested that ACP had behaved unusually on March 11-12, April 4-5, and April 20, 2015.

In the ionosphere (Fig. 3 and 4d), De Santis et al. (2017) found a very evident disturbance of geomagnetic field on April 14, 2015 by analysing the Swarm satellite data along the night orbital tracks. Investigating the daytime TEC time series over the seismogenic zones, Li et al. (2016) observed that the TEC had decreased 14d and 6d before the Gorkha earthquake with a duration of 6-8 h. Oikonomou et al. (2016) detected some enhancements of ionospheric diurnal TEC variations appearing 1-11 days before the Gorkha earthquake. Ulukavak et al. (2019) suggested that the positive ionospheric TEC anomaly, observed on April 22 (day-time) and April 23 (night-time), 2015, might be related to the Gorkha earthquake in that the space weather conditions and geomagnetic activity were quite in these days. Ouzounov et al. (2021) also found a strong night-time negative TEC anomaly occurring on April 21, and a strong night-time positive anomaly appearing on April 24, 2015. Besides, Tang and Yuan (2017) found significant ionospheric TEC fluctuations and multi-dimensional structures appearing around the Gorkha earthquake, and coseismic ionospheric disturbances appearing to the northeast and northwest of epicenter 10-20

minutes about after the mainshock. VTEC rising before and dropping after the mainshock directly above the faults and VTEC enhancing 14 minutes about prior to the Dolakha earthquake were observed by using GPS observations (He and Heki 2017).

210 Night-time VLF signal transmitted from Australia and received in Allahabad, India (25.4º N, 81.9º E) showed that fluctuation of VLF appeared 1 d before both the Gorkha earthquake and the Dolakha earthquake (Maurya et al. 2016; Phanikumar et al. 2018). VLF/LF signals in the night-time transmitted from Sakhalin Island and received in Varanasi, India (25.3º N, 82.9º E) had exhibited significant depression from April 21 to April 23, while that transmitted from south India and received in Varanasi, India displayed obvious decrease from April 20 to April 24, 2015 (Ouzounov et al. 2021).
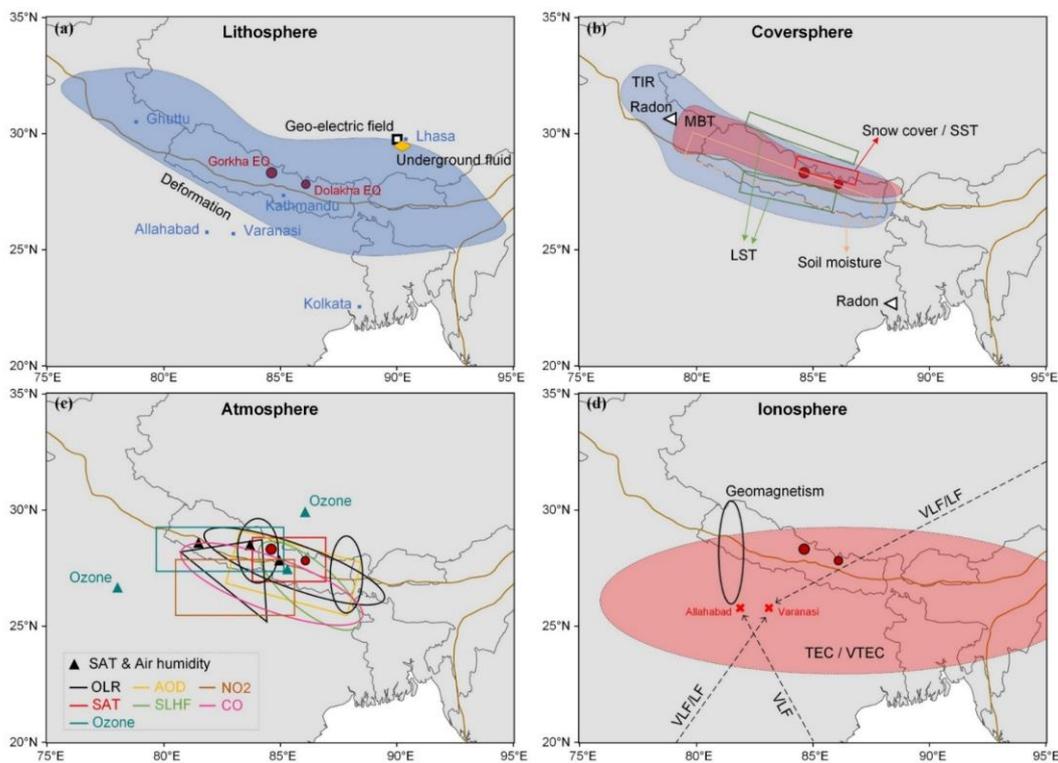
215

Figure 4: The spatial distribution of multiple anomalies in four geospheres before, during and after the Gorkha earthquake and Dolakha earthquake in 2015. The geographical locations of the stations were marked for the anomalies recorded by the ground station, the areas of significant anomalies with detailed description were marked for the anomalies observed by satellites. In Fig. 4a, the blue area only represents the long-term and large-scale deformation area, not the short-term deformation anomaly. In Fig.4d, the red area represents the

220 northern part of the conjugate ionospheric anomalies.

3.2 Aggregative characteristics of multiple anomalies

As shown in Fig.3 and Fig.4, the parameters of the lithosphere, such as deformation, geoelectric field, underground water temperature and level, could be the first to change at long-term scale. The long-period surface deformation was mainly concentrated in the boundary zone between the Qinghai-Tibet Plateau and the Indian plate, which basically covered the whole

225   Himalayan region as a stripe. The observation sites for geoelectric anomalies and underground fluids locate in Lhasa, Tibet, which is farther northeast of the epicenters but falls inside the primary deformation zone.

The anomalies in the coversphere mainly appeared 20d before, and lasted until more than 10d after the Gorkha mainshock. A few parameters, such as MBT, appeared repeatedly before and disappeared after the Dolakha aftershock. These anomalies were mainly concentrated in a strip region along the southern foothills of the Himalayas. TIR anomaly was the most extensive,

230   while the other anomalies in coversphere were generally occurred inside the region of TIR anomaly. Snow cover and snow surface temperature anomalies occurred at high altitudes close to the epicenter, while SSM anomalies and LST anomalies occurred at lower altitude regions. Stations for detecting radon gas in soil and in underground water were located in the southeast India (Kolkata) and northwest India (Ghuttu), which was far away from the two epicenters.

In the atmosphere, the earliest anomalies were thermal parameters, such as SAT, OLR and ACP, following by other gas

235   anomalies occurring within 20d before the Gorkha earthquake. Most of the gas anomalies only lasted until the Dolakha earthquake, while the thermal parameter anomalies continued until more than 10d after the Dolakha earthquake. Except for the ozone stations locating far away from the epicenters, the other atmospheric anomalies were generally distributed in the belt region to the south of the Himalayas. These atmospheric anomalies showed strong spatial aggregation and corresponded well to the union scope of seismic anomalies in lithosphere and coversphere.

240   The ionospheric anomaly appeared 13d before the Gorkha earthquake and displayed intermittent peak values. Its appearance was significantly later than that in the lower geospheres. From 3d before the Gorkha earthquake to the coseismic day, significant ionospheric anomalies frequently appeared. Subsequently, electronic anomalies and electromagnetic anomalies appeared intensively 3d before and on the date Dolakha shocking, and then disappeared. Due to the scattered distribution of GNSS stations and sparse orbits of electromagnetic satellites, the spatial range of ionospheric anomalies was relatively broad,

245   which lead to some distant stations that detected also ionospheric anomalies cannot be displayed in Fig. 4.

4 Crustal stress field alteration in Nepal Himalayas

4.1 Numerical simulation of CSFA

It is well established that tectonic earthquake is attribute to the gradual accumulation and localized concentration of crustal stress. The CSFA before the 2015 Gorkha earthquake in Nepal is critical to understand the observed seismic anomalies and

250   unravel the corresponding LACI coupling mechanisms. In this work, considering the hypocentres at a depth of approximately 15 km, a refined 3D geological model with detailed information of main faults and strata in the study area was constructed based on the existing data and reported studies (Decelles et al., 1998, 2001; Lavé and Avouac 2001; Avouac 2003; Bollinger et al., 2004; Sapkota et al., 2013), which is shown in Fig. 5. The major tectonic faults in Nepal (including MFT, MBT', MCT, and MHT) and the Yarlung Zangbo Suture Zone (YZSZ) to the north of Nepal Himalayas are built in the 3D model. The

255   surface topography was reconstructed by using DEM data (ASTER GDEMv3) with resolution downscaled to 500m. By using

a 3D finite element method (ANSYS software), the accumulation of equivalent stress (named also von Mises stress) caused by tectonic movement in the Nepal Himalayas over the last 500 years was numerically simulated referring to the average annual ground surface velocity fields from 1990 to 2015 (Gan et al., 2007; Ader et al., 2012; Kreemer et al., 2014; Zheng et al., 2017). The upper and lower parts of the Moho surface was considered to be elastic and viscoelastic, respectively (Zhao et al., 2017; Tian et al., 2020). The physical parameters used were referred to existed studies (Castaldo et al., 2016; Zhao et al., 2017; Wang and Fialko, 2018; Tian et al. 2020), and the nonlinear frictional contact was applied to the faults with its friction coefficient being set as 0.4 (Luo and Liu 2010). Self-weighing of elements was considered due to the large differences in surface topography in Nepal Himalaya. The boundary conditions of model were constrained by the velocity fields and the bottom domain is free horizontally but fixed vertically.
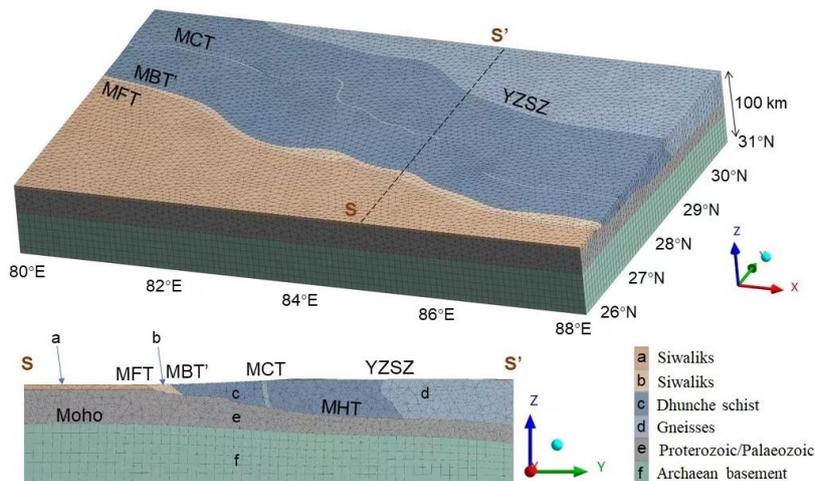
265

Figure 5: 3D geometrical model of geological structure in Nepal and its nearby areas. MFT, MBT', MCT and MHT mean the same as before, while YZSZ means Yarlung Zangbo suture zone. The X-axis is west-east, the Y-axis is south-north, and the Z-axis is bottom-up. For each domain, the density values (ρ), Young's Modulus (E), and Poisson's ratio (ν) were reported as: $\rho = 2550$, $E = 20$, and $\nu = 0.25$ in strata a and b; $\rho = 2700$, $E = 40$, and $\nu = 0.25$ in strata c and d; $\rho = 2700$; $E = 70$, $\nu = 0.25$ in strata e; $\rho = 2700$, $E = 170$, $\nu = 0.25$, and coefficient of viscosity = 10^{20} Pas in strata f.

The equivalent stress (von Mises stress) suggests that the rock will get yield if the second invariant of the deviatoric stress reach some critical value (Jaeger et al., 2009), which could be used to reflect the crust stress background. An increment in the equivalent stress will accelerate the failure of solid medium, while a decrement will prevent the solid medium from yielding. The 3D distribution of computed equivalent stress in the volume of the geological model was presented in Fig. 6a. Particularly, the computed equivalent stress on the ground surface (Fig. 6b) as well as that on the MHT structural surface (Fig. 6c) were sectioned and analysed. In order to better show the equivalent stress change at different depths, the equivalent stress distribution in two specially selected sections (A and B) were shown in Fig. 6d and Fig. 6e, respectively.
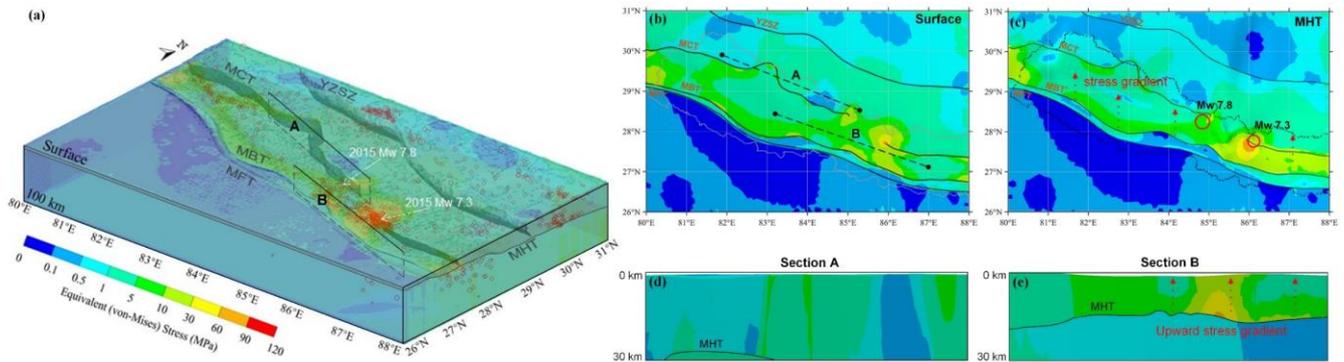
Figure 6: The spatial distribution of equivalent stress in a 3D perspective (a), on the surface (b) and MHT (c), and on section A (d)
280 **and section B (e).** Red circles in (a) represent the hypocentres of seismic activities (Mw ≥2.5, 1921–2022) from USGS.

Obviously, the stress field varied a lot with the tectonic structures (Fig. 6a). The high-stress build-up was mainly associated
with the MBT' and MCT, shaped with a narrow belt along the faults, which coincides with the belt-shaped seismicity illustrated
in Fig. 1 and reported by Pandey et al. (1999). Particularly, remarkable stress accumulation, with a maximum stress of up to
90–120 MPa, appeared around the hypocentres of the 2015 M_w 7.8 mainshock and its largest aftershock (M_w 7.3) (Fig. 6c),
285 which might have reached the yield strength of local rock mass. In addition, both the magnitudes and areas of the concentrated
stress on the ground surface (Fig. 6b) were relatively smaller than that on the MHT fault plane (Fig. 6c), suggesting an overall
upward stress gradient between the MHT and ground surface. Fig. 6e shows that the maximum stress accumulation zone
located at the depth of MHT. The stress distribution was relatively uniform with low value in the deep part under MHT, and
the stress in the shallow part shows a clear trend decreasing from the MHT plane to ground surface (resulting an upward stress
290 gradient), which can be observed in section B (Fig. 6e). Moreover, the stress distributions at north-western of Nepal is relatively
lower than that at southern and eastern regions, suggesting an overall northward stress gradient in Nepal. In short, the CSFA
in the Nepal Himalayas was mainly determined by the tectonic structures, and displayed inhomogeneous spatial pattern in 3D
space. It is expected that CSFA in the Nepal Himalayas was closely related to the multiple seismic anomalies before the
occurrence of 2015 Nepal earthquake sequence.

295 **4.2 Response chains of CSFA**

Rock mechanics have demonstrated that many physical properties of rocks, such as geological structure, physical temperature,
acoustic emission, electric property, and even electromagnetic radiation, will change with the increasing of additional stress.
Since most of them appeared or occurred remarkably before the final rock failure, the significant variations of local stress are
considered as their sources or roots. However, the change in ground stress near the Earth's surface is merely in the order of
300 several MPa (Liao et al., 2003; Yukutake et al., 2010; Hasegawa et al., 2012), which is substantially smaller than that at depths
of 10–45 km, where approximately 85% of destructive earthquakes occurred with considerable stress enhancement. Thus, how
to understand the spatial gap between the observed anomalies near and above ground surface and the significant stress changes

at hypocentres (depth of 15km) of Nepal earthquake is very critical. In addition, an increase in seismicity rate was found 3-4 days prior to the mainshock of 2015 Nepal earthquakes (Huang et al. 2016), which means that local stress had changed

305 significantly during this period. However, the reported seismic anomalies associated with the Nepal earthquakes (Fig. 3 and 4) were generally observed or appeared several to tens of days before the occurrence of earthquakes; thus, the physical process without significant stress change is expected to be responsible for the anomalies. Therefore, a stress-associated physical process considering both the spatial and temporal gaps should be further explored.

Figure 6 shows that the crustal stress distributing on and above the MHT fault plane, especially corresponding to the Nepal,

310 was highly concentrated and unevenly distributed. Thus, as the crust stress build up locally, the area of high-grade metamorphic rocks schist and gneisses (Fig. 5), which contain numerous peroxy bonds or oxygen defects (Freund et al., 2002, Freund, 2007), would have produced massive positive charge carries (or positive holes, P-holes in brief) (Freund, 2010). The P-holes are to flow out from the source area to upper portions of the crust with the stress gradients acting as the driving force (St-Laurent et al., 2006). The 3D distribution of uneven stress accumulation in Fig. 6a indicates that the regional stress gradient developed

315 vertically from MHT to ground surface and horizontally from south to north, which determined that the produced P-holes were able to transmit upward and northward along the stress gradient from the hypocenter zone. Therefore, the ground surface above the high stress concentration zone could be the core area of P-holes aggregation. The combined analysis of the numerical simulation and P-hole theory shows that the CSFA response chain of '*CSFA—P-hole producing and flowing down stress gradients—surface P-hole accumulating*' existed before the Nepal earthquakes in 2015.

320 In laboratory experiments, enhanced TIR radiation was observed on the free end of compressed rock using a spectra-radiometer, which was considered to be caused by P-holes recombination as it reaches to and recombine on the rock surface (Freund 2007). Theoretical analysis and practical observation show that continuous P-holes accumulation on ground surface will produce additional electric field and lead to sequential anomalies in the atmosphere and ionosphere (Freund et al., 2011). In addition, the aggregation of P-holes in the shallow surface of rock volume is bound to generate a regional electric field

325 (Freund 2007), and the lattice ions in the rock volume will shift under the action of the additional electric field. Thus, the microwave dielectric constant of rock material (Mao et al., 2020) get reduced, which is also confirmed by laboratory observation of the dielectric change in non-stressed volume during rock loading (Mao et al., 2020, 2021).

Therefore, as massive CSFA-activated P-holes migrate upward and reach to ground surface or mountain peaks, there are at least three different response chains with homologous physics. The first is the change of microwave permittivity caused by the

330 electric field enhancement in shallow rock volume, the second is the additional infrared radiation emitted during the recombination of P-holes on ground surface, and the third is the atmospheric ionization and sequential productions of atmospheric and ionospheric anomalies caused by atmospheric electric field (AEF) enhancement and upward ionic motion.

5 CSFA-based rooting and LCAI Coupling analysis

As shown in Fig. 3 and Fig. 4, the seismic anomalies appeared in the four geospheres displayed an obvious upward evolution
335   as the mainshock approaching, and also exhibited strong spatial aggregation and great correspondence to the seismogenic zone.
Nevertheless, there still existed some inconsistency in the abnormal behaviours of different anomalies, such as the rise, fall or
fluctuation behaviours in time domain, and the distributions of different anomalies did not overlap fully each other in space
domain. In Sec. 4, CSFA is identified as the fundamental driver of the seismic anomalies and three potential stress response
chains are presented. The reported multi-parameter seismic anomalies should be further screened and rooted, only those
340   anomalies matching perfectly the homologous physics in CSFA and behaved spatio-temporal consistency can be retained and
considered as reliable seismic anomalies with potential earthquake precursor meanings.

The ionospheric anomalies appearing shortly before an earthquake are supposed to be potential precursors of an impending
earthquake. However, the preseismic ionospheric anomalies are always characterized by large scopes and long distances away
from the epicentres, even accompanied by conjugate phenomenon. Although a significant ionospheric anomaly could be
345   observed preceding an earthquake, it is difficult to determine the potential seismogenic area only depending on a single
ionospheric parameter. By analysing the spatio-temporal coincidence between the parameters in the same geosphere including
ionosphere through the DTS criterion, the unreliable seismic anomalies can be eliminated. From the top down to the bottom,
the anomalies with inconsistent physical mechanisms in different geospheres can be further excluded by analysing the possible
physical homology between the anomalies appeared in adjacent geospheres through LCAI coupling mechanism. Therefore,
350   the ionospheric anomaly can be rooted gradually down to the lithosphere and correlated with the CSFA firmly, and the potential
seismogenic zone can be identified, even the locked-in areas of crustal stress can be roughly ascertained.

5.1 Ionospheric anomalies

The ionospheric anomalies before the 2015 Nepal earthquakes have been summarized in Sec.3 and displayed in Fig. 4d. The
transmission path of the reported VLF/ELF abnormal signals (Ouzounov et al., 2021; Phanikumar et al., 2018; Maurya et al.,
355   2017) passed over the stress concentration area shown in the simulation results, and the moments of VLF/ELF anomalies
appearance were also concentrated in the very short moment before the mainshock. Therefore, the reported VLF/ELF
disturbances can be preliminarily identified to satisfy the DTS criterion. However, it is generally considered that the upward
drift of ions (driving by CSFA induced additional electric field) from lower-atmosphere to the interface of upper atmosphere
and lower ionosphere would form a vertical current and participated into the global electrical circuit (Rycroft et al. 2008),
360   hence to impacts on the very low frequency (VLF) signals transmitting thorough the ionosphere. Whether the reported
VLF/ELF disturbances can be regarded as reliable earthquake precursor still requires further investigation of the spatio-
temporal characteristics and physical homology of atmospheric parameters.

The reported TEC/VTEC anomalies exhibited typical conjugate distribution (Li et al., 2016; Ouzounov et al., 2021;
Oikonomou et al., 2016), with the north part of the conjugated anormal region appearing in the Nepal Himalayas (in Fig. 4d).

365 We noticed the orbits of the satellites and the locations of GPS/GNSS stations, which were used for detecting TEC/VTEC anomalies, all passed over (He et al., 2017; Tang and Yuan 2017) or located in the stress concentration zone (Tang and Yuan 2017; Ulukavak et al., 2016). The abnormal geomagnetic signals detected by the Swarm mission (De Santis et al., 2017) appeared also near the west of the epicenter of Gorkha earthquake. Besides, these reported anomalies all appeared quite short before the shocking. However, the additional vertical electric field and electrostatic action of accumulated charges at the

370 ground-to-air interface would have caused the positive ions to move upward with fine particles of light mass and reduce the electron content in the bottom ionosphere, resulting in negative TEC anomaly (Freund 2011). Therefore, the negative TEC/VTEC anomaly (Li et al., 2016; Ouzounov et al., 2021) can be firstly retained. Like VLF/ELF anomalies, before the reported TEC/VTEC anomalies can be considered as a response of CSFA, the coupling mechanism between them and anomalies in lower altitude needs to be further validated.

375 **5.2 Atmospheric anomalies**

ACP will change once the ionization process start in the near-surface atmosphere. Therefore, it is reasonable that ACP anomalies (Ouzounov et al 2021) appeared first among all the atmospheric anomalies before the Gorkha earthquake. The decrease of air humidity and the increase of AOD are twin seismic phenomena in atmosphere. The occurrence of these two anomalies confirmed the increased concentration of nucleating particles in the low layer of atmosphere, which means that a

380 large number of ionizations had been produced in near-surface atmosphere and inevitably led to the rise of SAT (Jing et al., 2019; Hazra et al., 2017) and the drop of near-surface atmospheric electric field (unfortunately lack of in-situ observation). During the process of hydration or condensation, the phase of atmospheric molecules was transited from a free to a bound state, and additional latent heat was released (Jing et al., 2019). The atmospheric anomalies thus exhibited a scientifically correct temporal order as shown in Fig. 7. OLR reflects the total radiation energy (4-∞ μm) from ground surface, atmosphere

385 and clouds (Ohring et al., 1982), its enhancement could not be definitely contributed by the thermal anomalies in the atmosphere. From this perspective, the anomaly of OLR before the 2015 Nepal earthquakes (Ouzounov et al., 2021; Lu et al., 2016; Sun et al., 2017; Chakraborty et al., 2018) cannot be attribute sufficiently to the coupling process in the atmosphere. The reported change of carbon and nitrogen gas (Ganguly 2016; Phanikumar et al., 2018; Jing et al., 2019) might be owing to the surface cracks caused by local CSFA, but not directly correlated with any of the three response chains of CSFA, which tells

390 that the carbon and nitrogen anomalies cannot be coupled to ionospheric anomalies. Besides, based on the temporal characteristics of atmospheric anomalies, the reported decrease of TEC 14d before the mainshock reported by Li et al., (2016) should be denied due to its earlier occurrence than the top atmospheric anomaly.
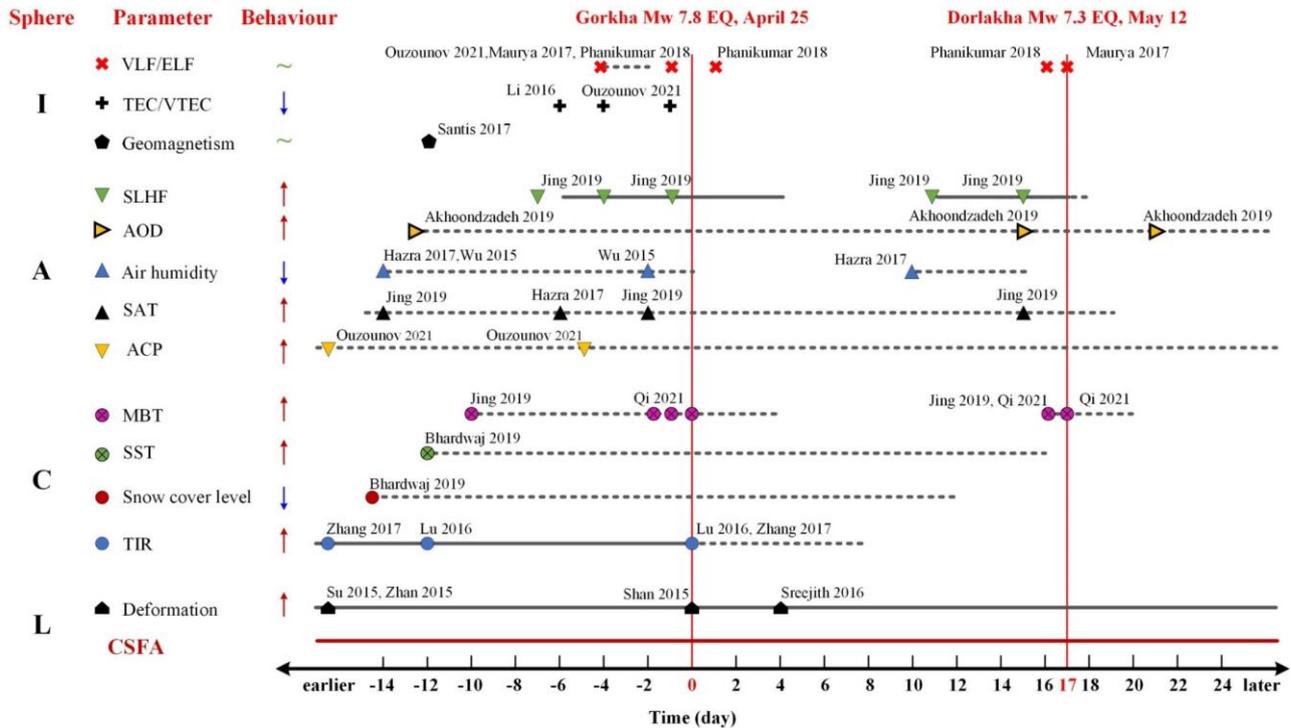
Figure 7: The temporal distribution of screened seismic anomalies, which could be attributed to CSFA and stress-activated P-holes. ↑ denotes positive anomaly, while ↓ means negative anomaly, and ~ represents fluctuating or discrete anomaly.

5.3 Coverspheric anomalies

TIR radiation was observed not only on the fracturing surface (3.6-14 μm) (Wu et al., 2000, 2006a, 2006b; Liu et al., 2004; Ma et al., 2008; Zhou et al., 2019) but also on the free end (8-12.5 μm) (Freund et al. 2011) of the compressed rock using infrared imager or spectra-radiometer in laboratory, which could be attributed partly to a synergic physics (Liu et al., 2021) including the recombination of P-holes (Freund 2007). TIR anomalies (Lu et al., 2016; Zhang et al., 2017) were the earliest to be observed by satellites (between 8-12.5 μm) before the Gorkha earthquake. The reported MBT anomalies were more concentrated than the TIR anomalies in space (Jing et al., 2019; Qi et al., 2021). In particular, positive abnormal MBT stripes not only behaved in temporal consistency with the repeated process of earthquake preparation and eruption, but also exhibited a significant topographic consistency with the north-south elevation profile of the Himalayas (Qi et al., 2021). The recombination of P-holes might have started rightly and led to TIR anomalies as soon as it reached to ground surface, while the enhancement of MBT only appeared when and where the P-holes got sufficiently accumulated as the major events approaching. Hence the TIR anomaly could have occurred earlier than the MBT anomaly. Besides, the snow cover north near the Gorkha epicenter got an accelerated melting, which was attributed to the strengthened thermal gradient between snow pack

410 and charges layer and resulted in an increase in SST (Bhardwaj et al., 2019). The snow cover anomaly overlapped the MBT anomaly in space, which could be served as the responses of CSFA induced P-holes aggregation. All the anomalies mentioned above occurred in the high stress concentration zone as that revealed by numerical simulation. Therefore, same as the atmospheric anomalies, they can all act as aftereffects of P-holes aggregation.

However, SSM increment at the epicenter regions (Jing 2019) was contradict with the positive thermal anomalies (such as TIR

415 and MBT anomalies). The positive LST anomaly (Shah et al., 2016; Baral et al., 2016) was far from the spatial aggregation zone where most anomalies clustered together, and the negative LST anomaly appeared to the north of the epicenter (Chen et al., 2020) seemed to be related to the tensile behaviour of local rock mass, rather than linked to the compressive stress. Therefore, we are unwilling to accept the reported SSM and LST anomalies as seismic anomaly with homologous physics in CSFA. Radon emanation mainly occurred in Kolkata, India (22.6º N, 88.4º E) and Ghuttu, India (30.5º N, 78.8º E) (see Fig.

420 4), where are 700 km away from the mainshock epicenter (Deb et al., 2016; Kumar et al., 2017) and obviously separated from the rest of the seismic anomalies. The reported radon emanation could be linked to the regional tectonic movement but not definitely to the very localized CSFA in the seismogenic zone.

5.4 Lithospheric anomalies

The pre-seismic and co-seismic displacement fields observed by GPS and InSAR technology showed that the crustal

425 deformation before the Nepal earthquakes was featured by a striped compression zone (Shan et al., 2015; Sreejith et al., 2016), which fit well with the simulated results in Fig. 6. The coincidence between the deformation and the high stress concentration on earth surface further indicates the reliability of the simulation results. According to the three response chains of CSFA, the upward migration of P-holes from the highly compressed seismogenic zone would have inevitably disturbed the amount of charged particles and the conductivity of ground soil or shallow rocks, thus changing the geoelectric field (Xi et al.,2016).

430 However, we are not able to accept the reported geoelectric anomaly in the LCAI coupling in that the location of geoelectric station is far away from where the seismic anomalies appeared in coversphere and atmosphere. Although the variation of underground water anomalies, including temperature (Yang et al., 2016) and water-level (He et al., 2017; Ma and Huang 2017), might be caused by the CSFA, it might not directly interact with the compressive stress (Fig. 6) in that the observation location of underground water was almost separated from the principal compression region (Fig.4a). Hence, the reported underground

435 water anomalies are considered as non-homologous in this study.

5.5 Discussion on the homologous physics

Finally, the rootable seismic anomalies of multiple geospheres with homologous physics in CSFA as local crust stress accumulation are reached. The temporal process of the screened-out seismic anomalies being scientifically associated with the 2015 Nepal earthquake sequence is shown in Fig. 7. To better understand the spatio-temporal process of the LCAI coupling,

440 the spatial evolution of the retained rootable seismic anomalies is visualized in a 3D manifold space (Fig. 8).
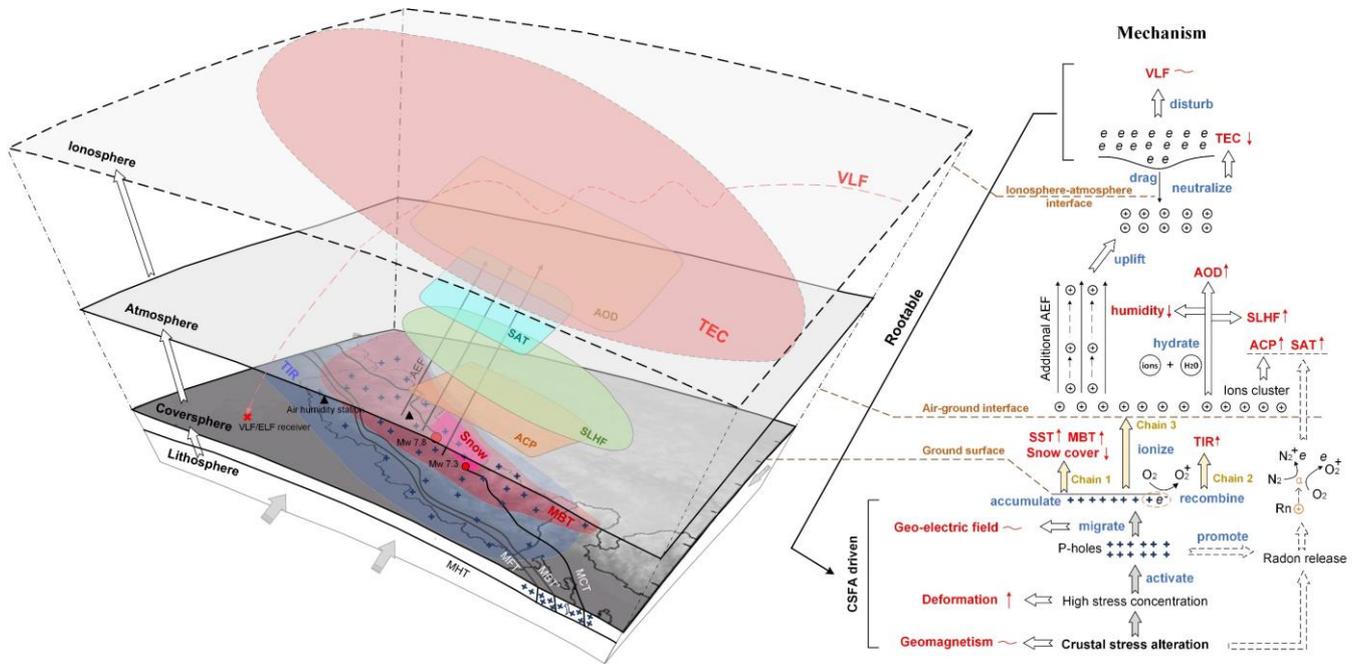
Figure 8: The integrated framework of rootable seismic anomalies as well as the evolution of LCAI coupling in a 3D manifold space. Line arrows and dashed arrows tell the coupling actions have been verified and not been proved, respectively.

The 3D numerical simulation shows the detailed pattern of CSFA as well as a high degree of local stress concentration in the
445   study area before the earthquake. The appearance of MBT anomalies indicates that the surface microwave dielectric did reduce, which confirms the existence of the first response chain of CSFA. Surface TIR anomalies indicate that the existence of the second response chain, while the atmospheric and ionospheric anomalies confirmed the third response chain of CSFA, as in Fig.8. The three stress response chains coexisted before the Nepal earthquake sequence in 2015, which shared the homologous physics in CSFA.

450   Freund et al. (2002, 2009, 2011) believe that P-holes are mobile and capable of flowing down stress gradients into an unstressed rock mass and finally accumulating on a distant rock surface, thus leading to sequential productions of anomalies in the atmosphere and ionosphere. Based on thorough investigation of geological and structural conditions, the 3D numerical simulation in this study uncovered the source, the path and the destination of P-holes generation, transmission and aggregation. Pulinets et al. (Pulinets and Boyarchuk 2004; Pulinets 2009) believes that the released radon gas due to CSFA will also give

455   rise to multiple seismic anomalies. Unfortunately, there was no radon observation site found falling in the stress concentration zone given by the simulation results, and the radon-driven chain cannot be proved for the Nepal earthquakes in 2015. However, it does not mean that radon induced seismic anomalies did not actually exist before the Nepal earthquakes sequence, it might work if available data is found in the stress concentration zone. Besides, in another of our studies, the hydrothermal anomalies before the 2009 L'Aquila earthquake in Italy showed evident quasi-synchronous features, which indicated a geosphere coupling

460   process (Wu et al., 2016). No matter whether the seismic anomaly is caused by P-holes or/and by the decay of radon, or by the

hydrotherm, it could all be rooted to regional CSFA as well its local blocking. Since the existence of P-holes can stimulate the release of radon to a certain extent (Freund 2010), the two theories are not isolated from each other but compatible with the CSFA-driven framework.

6 Conclusions

465   In this study, a large number of literatures on the seismic anomalies possible related with 2015 Nepal earthquake sequence were collected and reviewed carefully. A spatio-temporal diagram of the reported seismic anomalies was preliminary constructed under the umbrella of LACI coupling paradigm, which exhibits an obvious temporal sequence of developing upward as the mainshock approaching and a strong spatial aggregation corresponding to the seismogenic zone.

    By numerically simulating the equivalent stress accumulation over the past 500 years, inhomogeneous CSFA along the faults
470   and around the hypocentres of 2015 Nepal earthquake sequence are illustrated clearly. The joint analysis of crust stress simulation and tectonic environment shows that there existed a chain of '*CSFA—P-hole producing and flowing down stress gradients—surface P-hole accumulating*' before the Nepal earthquakes in 2015. The regional CSFA as well as its local blocking can be regarded as the root of seismic anomalies in the Nepal Himalayas. Three different stress response chains with homologous physics in CSFA were theoretically summarized, i.e., the decrease of microwave dielectric caused by electric
475   field enhancement in shallow rock volume, the additional infrared radiation due to P-holes recombination on ground surface, and the atmospheric ionization together with sequential anomalies caused by atmospheric electric field enhancement due to P-holes accumulation.

    Accordingly, the preliminary obtained spatio-temporal diagram of reported seismic anomalies was screened and rooted retroactively with the homologous physics in CSFA. Finally, an integrated LCAI coupling framework with strict space-time
480   coincidence and the homologous physics in CSFA was presented, and a synergic chain of *CSFA—P-hole activation, migration and aggregation—seismic anomalies* associated with the Nepal earthquakes in 2015 was proposed and verified. Furthermore, the spatio-temporal evolutions of the rootable seismic anomalies are visualized in a 3D manifold space to better understanding the LCAI coupling process. This study and the results are of scientific meanings for searching earthquake precursors and for reaching earthquake prediction in the near future.

485   However, the change of near surface vertical AEF, which is an important atmospheric parameter that could be directly respond to the P-holes aggregation on ground surface and its subsequent electric effect, have not been reported after the 2015 Nepal earthquake sequence. The radon observation and the induced seismic anomaly in the local stress concentration area, which is very important to establish another coupling process related to CSFA, have not been reported so far for the lack of effective observation sites. To further enhance the synergic method of LCAI coupling of homologous physics for screening seismic
490   anomalies and searching earthquake precursors, some other parameters in the lithosphere being able to reflect the propagation of P-holes should be carefully investigated. Especially, the observation on vertical AEF as well as the investigation to its seismic disturbance should be fully addressed.

Data availability

All data can be provided by the corresponding authors upon request.

Author contributions

LW, YQ and WM designed the framework of the manuscript; YQ wrote the manuscript draft; LW and WM carried out the mechanical analysis and polished the manuscript; WM, YD, JL, BP, and BX completes the visualization. All authors have read and agreed to the published version of the manuscript.

Competing interests

The authors declare that they have no conflict of interest.

Financial support

This work was supported by the Key Program of National Nature Science Foundation of China (41930108), National Nature Science Foundation of China (42101394), and Nature Science Foundation of Hunan Province, China (2021JJ40725).

References

Ader, T., Avouac, J. P., Liu-Zeng, J ., Lyon-Caen, H., Bollinger, L., Galetzka, J., Genrich, J., Thomas, M., Chanard, K., Sapkota, SN., Rajaure, S., Shrestha, P., Ding, L., and Flouzat, M.: Convergence rate across the Nepal Himalaya and interseismic coupling on the Main Himalayan Thrust: Implications for seismic hazard. J. Geophys. Res. Solid. Earth., 117, B4, https://doi.org/10.1029/2011JB009071, 2012.

Akhoondzadeh, M., and Chehrebargh, F.J.: Feasibility of anomaly occurrence in aerosols time series obtained from MODIS satellite images during hazardous earthquakes, Adv. Space. Res., 58, 890-896, doi: 10.1016/j.asr.2016.05.046, 2016.

Akhoondzadeh, M., De Santis, A., Marchetti, D., Piscini, A., and Jin, S.: Anomalous seismo-LAI variations potentially associated with the 2017 Mw = 7.3 Sarpol-e Zahab (Iran) earthquake from Swarm satellites, GPS-TEC and climatological data, Adv. Space Res., 64, 143-158, 10.1016/j.asr.2019.03.020, 2019.

Avouac, J. P.: Mountain building, erosion, and the seismic cycle in the Nepal Himalaya, Adv. Geophys., 46, 1-80, https://doi.org/10.1016/S0065-2687(03)46001-9 ,2003.

Avouac, J., Meng, L., Wei, S., Wang, T., and Ampuero, J.: Lower edge of locked Main Himalayan Thrust unzipped by the 2015 Gorkha earthquake, Nat. Geosci., 8, 708, 10.1038/NGEO2518, 2015.

Baral, S. S., Sharma, K., Saraf, A. K., Das, J., Singh, G., Borgohain, S., and Kar, E.: Thermal anomaly from NOAA data for the Nepal earthquake, Curr. Sci., 110, 150, 2016.

520 Bhardwaj, A., Singh, S., Sam, L., Bhardwaj., A., Martin-Torres, F. J., Singh, A., Kumar, R.: MODIS–based estimates of strong snow surface temperature anomaly related to high altitude earthquakes of 2015, Remote Sens. Environ., 188, 1-8, https://doi.org/10.1016/j.rse.2016.11.005, 2017.

Bilham, R.: Earthquakes in India and the Himalaya: tectonics, geodesy and history, Ann. Geophys., 47, doi: 10.4401/ag-3338, 2004.

525 Bollinger, L., Avouac, J. P., Cattin, R., and Pandey, M.R.: Stress buildup in the Himalaya, J. Geophys. Res. Solid Earth, 109, 1-8, https://doi.org/10.1029/2003JB002911, 2004.

Castaldo, R., De Novellis, V., Solaro, G., Pepe, S., Tizzani, P., De Luca, C., Bonano, M., Manunta, M., Casu, F., Zinno, I., and Lanari, R.: Finite element modelling of the 2015 Gorkha earthquake through the joint exploitation of DInSAR measurements and geologic-structural information, Techno., 714, 125-132, 10.1016/j.tecto.2016.06.037, 2017.

530 Chakraborty, S., Sasmal, S., Chakrabarti, S. K., and Bhattacharya, A.: Observational signatures of unusual outgoing longwave radiation (OLR) and atmospheric gravity waves (AGW) as precursory effects of May 2015 Nepal earthquakes, J. Geodyn., 113, 43-51, 10.1016/j.jog.2017.11.009, 2018.

Chen, S., Liu, P., Feng, T., Wang, D., Jiao, Z., Chen, L., Xu, Z., and Zhang, G.: Exploring Changes in Land Surface Temperature Possibly Associated with Earthquake: Case of the April 2015 Nepal Mw 7.9 Earthquake, ENTROPY, 22,
535 10.3390/e22040377, 2020.

De Santis, A., Balasis, G., Pavon-Carrasco, F. J., Cianchini, G., Mandea, M.: Potential earthquake precursory pattern from space: The 2015 Nepal event as seen by magnetic swarm satellites.: Earth Planet. Sci. Lett., 461, 119–126, doi: 10.1016/j.epsl.2016.12.037, 2017.

Deb, A., Gazi, M., and Barman, C.: Anomalous soil radon fluctuations - signal of earthquakes in Nepal and eastern India
540 regions, Earth Syst. Sci., 125, 1657-1665, 10.1007/s12040-016-0757-z, 2016.

DeCelles, P. G., Gehrels, G. E., Quade, J., Ojha, T. P., Kapp, P. A., and Upreti, B. N.: Neogene foreland basin deposits, erosional unroofing, and the kinematic history of the Himalayan fold-thrust belt, western Nepal, Geol. Soc. America Bull., 110, 2-21, https://doi.org/10.1130/0016-7606, 1998.

Decelles, P. G., Robinson, D. M., Quade, J., Ojha, T. P., Garzione, C. N., Copeland, P., and Upreti, B. N.: Stratigraphy,
545 structure, and tectonic evolution of the Himalayan fold-thrust belt in western Nepal, Tectonics, 20, 487-509, https://doi.org/10.1029/2000TC001226, 2001.

Dey, S., Singh, R. P.: Surface latent heat flux as an earthquake precursor, Nat. Hazards Earth Sys. Sci., 3, 749-755, https://doi.org/10.5194/nhess-3-749-2003, 2003.

Freund, F. T., Kulahci, I. G., Cyr, G., Ling, J., Winnick, M., Tregloan-Reed., J. and Freund., M. M.: Air ionization at rock
550 surfaces and pre-earthquake signals, J. Atmos. Solar-Terrestrial Phys., 71, 1824–1834, https://doi.org/10.1016/j.jastp.2009.07.013, 2009.

Freund, F. T., Takeuchi, A and Lau, B.: Electric currents streaming out of stressed igneous rocks – a step towards understanding pre-earthquake low frequency EM emissions, Phys., Chem., Earth, 31, 389-396, https://doi.org/10.1016/j.pce.2006.02.027, 2006.

555 Freund, F. T.: Charge generation and propagation in igneous rocks, J. Geodynamics, 33, 543–570, https://doi.org/10.1016/S0264-3707(02)00015-7, 2002.

Freund, F. T.: Pre-earthquake signals: Underlying physical processes, J. Asian Earth Sci., 41. 383–400, https://doi.org/10.1016/j.jseaes.2010.03.009, 2011.

Freund, F. T.: Pre-earthquake signals—Part I: Deviatoric stresses turn rocks into a source of electric currents, Natural Hazards
560 Earth Syst. Sci., 7, 535–541, https://doi.org/10.5194/nhess-7-535-2007, 2007.

Freund, F. T.: Toward a unified solid state theory for pre-earthquake signals. Acta Geophysica, 58, 719-766, https://doi.org/10.2478/s11600-009-0066-x, 2010,

Gan, W. J., Zhang, P. Z., Shen, Z. K., Niu, Z. J., Wang, M., Wan, Y. G., Zhou, D. M., and Cheng, J.: Present-day crustal motion within the Tibetan Plateau inferred from GPS measurements. J. Geophys. Res. Solid. Earth., 112, B8,
565 https://doi.org/10.1029/2005JB004120, 2007.

Ganguly, N. D.: Atmospheric changes observed during April 2015 Nepal earthquake, J. Atmos. Sol.–Terr. Phy., 140, 16-22, https://doi.org/10.1016/j.jastp.2016.01.017, 2016.

Genzano, N., Aliano, C., Corrado, R., Filizzola, C., Lisi, M., Mazzeo, G., Paciello, R., Pergola, N., and Tramutoli, V.: RST analysis of MSG-SEVIRI TIR radiances at the time of the Abruzzo 6 April 2009 earthquake, Nat. Hazards Earth Sys. Sci., 9,
570 2073-2084, https://doi.org/10.5194/nhess-9-2073-2009, 2009.

Gokhberg, M. B., Buloshnikov, A. M., Gufeld, I. L. and Liperovsky, V. A.: Resonance phenomena at seismo-ionospheric interaction, Izv. AN SSSR, Fizika Zemli, 6, 5-8, 1985.

Guo, Z., Gao, X., Yao, H., Li, J., and Wang, W. M.: Midcrustal low-velocity layer beneath the central Himalaya and southern Tibet revealed by ambient noise array tomography, Geoche., Geophy., Geosys., 10, 5, https://doi.org/10.1029/2009GC002458,
575 2009.

Hasegawa, A., Yoshida, K., Asano, Y., Okada, T., Iinuma, T., and Ito, Y.: Change in stress field after the 2011 great Tohoku-Oki earthquake, Earth Planet. Sci. Lett., 355, 231-243, 10.1016/j.epsl.2012.08.042, 2012.

Hayakawa, M., Izutsu, J., Schekotov, A., Yang, S., Solovieva, M., and Budilova, E.: Lithosphere–Atmosphere–Ionosphere Coupling Effects Based on Multiparameter Precursor Observations for February–March 2021 Earthquakes (M~7) in the
580 Offshore of Tohoku Area of Japan, Geosci., 11, 481, 10.3390/geosciences11110481, 2021.

Hazra, P., De, S. S., Paul, S., Guha, G., and Ghosh, A.: Thermal Anomalies Around the Time of Nepal Earthquakes M 7.8 April 25, 2015 And M 7.3 May 12, 2015, Int. J. Geotech. Eng., 8, 58-73, 10.4018/IJGEE.2017010104, 2017.

He, A., Fan, X., Zhao, G., Liu, Y., Singh, R., P., and Hu, Y.: Co–seismic response of water level in the Jingle well (China) associated with the Gorkha Nepal (Mw 7.8) earthquake, Tectonophysics, 714, 82-89,
585 https://doi.org/10.1016/j.tecto.2016.08.019, 2017.

He, L. M., and Heki, K.: Ionospheric anomalies immediately before Mw7. 0–8.0 earthquakes, J. Geophys. Res., Space Phys., 122, 8659-8678, https://doi.org/10.1002/2017JA024012, 2017.

He, M., Wu, L., Cui, J., Wang, W., Qi, Y., Mao, W., Miao, Z., Chen, B., and Sheng, X.: Remote sensing anomalies of multiple geospheres before the Wenchuan earthquake and its spatiotemporal correlations, Nat. Remote Sens. Bull., 24, 2020.

590 Huang, H., Meng, L., Plasencia, M., Wang, Y., Wang, L., and Xu, M.: Matched-filter detection of the missing pre-mainshock events and aftershocks in the 2015 Gorkha, Nepal earthquake sequence, Tectonophysics, 714, 71-81, 10.1016/j.tecto.2016.08.018, 2017.

Jaeger, J. C., Cook, N. G. W., and Zimmerman, R.: Fundamentals of rock mechanics, John Wiley & Sons, 2009.

Jing, F. and Singh, R. P.: Response of surface and atmospheric parameters associated with the Iran M 7.3 earthquake, IEEE J.
595 Sel. Topics Appl. Earth Observ. Remote Sens., 15, 5841-5852, 10.1109/JSTARS.2022.3188003, 2022.

Jing, F., Shen, X. H., Hong, S. Y. and Ouyang, X. Y.: The application of remote sensing technology to earthquake science research, Remote Sens. Land Res., 28, 2, 5-8, https://doi.org/10.6046/gtzyyg.2008.02.02, 2008.

Jing, F., Singh, R. P., and Shen, X.: Land–atmosphere–meteorological coupling associated with the 2015 Gorkha (M 7.8) and Dolakha (M 7.3) Nepal earthquakes, Geomatics, Natural Hazards Risk, 10, 1267-1284,
600 https://doi.org/10.1080/19475705.2019.1573629, 2019.

Kreemer, C., Blewitt, G., and Klein, E. C.: A geodetic plate motion and Global Strain Rate Model, Geochem, Geophy, Geosy., 15, 3849–3889, https://doi.org/10.1002/2014GC005407, 2014.

Kumar, N., Chauhan, V., Dhamodharan, S., Rawat, G., Hazarika, D., and Gautam, P. K. R.: Prominent precursory signatures observed in soil and water radon data at multi-parametric geophysical observatory, Ghuttu for M-w 7.8 Nepal earthquake,
605 Curr. Sci., 112, 907-909, 2017.

Kumar, S., Wesnousky, S. G., Rockwell, T. K., Briggs, R. W., Thakur, V. C., and Jayangondaperumal, R.: Paleoseismic evidence of great surface rupture earthquakes along the Indian Himalaya, J. Geophy. Res.: Solid Earth, 111, 10.1029/2004JB003309, 2006.

Kuo, C. L., Huba, J. D., Joyce. G., and Lee, L. C.: Ionosphere plasma bubbles and density variations induced by pre-earthquake
610 rock currents and associated surface charges, J. Geophys. Res., Space Phys., 116, https://doi.org/10.1029/2011JA016628, 2011.

Lavé, J., and Avouac, J. P.: Fluvial incision and tectonic uplift across the Himalayas of central Nepal, J. Geophys. Res.: Solid Earth, 106, 26561-26591, https://doi.org/10.1029/2001JB000359, 2001.

Li, W., Guo, J. Y., Yue, J. P., Yang, Y., Li, Z., and Lu, D. K.: Contrastive research of ionospheric precursor anomalies between Calbuco volcanic eruption on April 23 and Nepal earthquake on April 25, 2015, Adv. Space. Res., 57, 2141-2153, doi:
615 10.1016/j.asr.2016.02.014, 2016.

Liao, C. T., Zhang, C. S., Wu, M. L., Ma, Y. S., and Ou, M. Y.: Stress change near the Kunlun fault before and after the Ms 8.1 Kunlun earthquake, Geophy. Res. Lett., 30, 10.1029/2003GL018106, 2003.

Liperovskaya, E. V., Pokhotelov, O. A., Oleynik, M. A., Alimov, O. A., Pavlova, S. S., & Kharimenko, M.: Some effects in the sporadic E-layer of teh ionosphere before earthquakes, Fizika Zemli, 11, 86-88, 1994.

620 Liperovsky, V. A., Pokhotelov, O. A. and Shalimov, S. L.: Ionospheric precursors of earthquakes. Nauka, Moscow, Russia, 1992.

Liperovsky, V. A., Pokhotelov, O. A., Meister, C. V. and Liperovskaya, E. V.: Physical models of coupling in the lithosphere-atmosphere-ionosphere system before earthquakes. Geomagn. Aeronomy, 48, 795-806, https://doi.org/10.1134/S0016793208060133, 2008.

625 Liu, P. X., Liu, L. Q., Chen, S. Y., Chen, G. Q., and M, J.: An experiment on the infrared radiation of surficial rocks during deformation, Seismol Geol., 03, 502-511., https://doi.org/10.1007/BF02873097, 2004

Liu, X. X., Wu, L. X., Zhang, Y. B., and Mao, W. F.: Localized Enhancement of Infrared Radiation Temperature of Rock Compressively Sheared to Fracturing Sliding: Features and Significance, Front. Earth Sci., 9, 767, https://doi.org/10.3389/feart.2021.756369, 2021.

630 Luo, G. and Liu, M.: Stress evolution and fault interactions before and after the 2008 Great Wenchuan earthquake, Techno., 491, 127-140, 10.1016/j.tecto.2009.12.019, 2010.

Ma, J., Ma, S. P., Liu, P. X., and L. Q.: Thermal field indicators for identifying active fault and its instability from laboratory experiments (in Chinese). Seismol Geol., 30, 363-382, https://doi.org/10.3969/j.issn.0253-4967.2008.02.004,2008.

Ma, Y., and Huang, F.: Coseismic water level changes induced by two distant earthquakes in multiple wells of the Chinese
635 mainland, Tectonophysics, 694, 57-68, https://doi.org/10.1016/j.tecto.2016.11.040, 2017.

Mao, W. F., Wu, L. X., Liu, S. J., Gao, X., Huang, J. W., Xu, Z. Y., and Qi, Y.: Additional microwave radiation from experimentally loaded granite covered with sand layers: Features and mechanisms, IEEE Trans. Geosci. Remote Sens., 58, 5008–5022, https://doi.org/10.1109/TGRS.2020.2971465, 2020.

Mao, W.F., Wu, L.X., Xu, Y.Y., Lu, J.C., and Qi, Y.: Change in Diorite Microwave Dielectric Property at the Free End Upon
640 Compressive Stress Application to the Other End, IEEE. Trans. Geosci. Remote Sens., 60, 1-13, https://doi.org/10.1109/TGRS.2021.3125992, 2021.

Marchetti, D., De Santis, A., Shen, X. H., Campuzano, S. A., Perrone, L., Piscini, A., Di Giovambattista, R., Jin, S. G., Ippolito, A., Cianchini, G., Cesaroni, C., Sabbagh, D., Spogli, L., Zeren, Z. M. Huang, J. P.: Possible Lithosphere-Atmosphere-Ionosphere Coupling effects prior to the 2018 Mw= 7.5 Indonesia earthquake from seismic, atmospheric and ionospheric data.,
645 J. Asian Earth Sci.,188, https://doi.org/10.1016/j.jseaes.2019.104097, 2020.

Maurya, A. K., Venkatesham, K., Tiwari, P., Vijaykumar, K., Singh, R., Singh, A. K., and Ramesh, D. S.: The 25 Apr. 2015 Nepal earthquake: Investigation of precursor in VLF subionospheric signal, J. Geophys. Res.: Space Phys., 121, 10403–10416, https://doi.org/10.1002/2016JA022721, 2016.

Mencin, D., Bendick, R., Upreti, B. N., Adhikari, D. P., Gajurel, A. P., Bhattarai, R. R., Shrestha, H. R., Bhattarai, T. N.,
650 Manandhar, N., Galetzka, J., Knappe, E., Pratt-Sitaula, B., Aoudia, A., and Bilham, R.: Himalayan strain reservoir inferred from limited afterslip following the Gorkha earthquake, Nat. Geosci., 9, 533-537, 10.1038/NGEO2734, 2016.

Molchanov, O. A. and Hayakawa, M.: Generation of ULF electromagnetic emissions by microfracturing, Geophy. Res. Lett., 22, 3091-3094, https://doi.org/10.1029/95GL00781, 1995.

Ohring, G., and Gruber, A.: Satellite Radiation Observations and Climate Theory, Adv. Geophys., 25, 237–304,
655 https://doi.org/10.1016/S0065-2687(08)60175-2, 1983.

Oikonomou, C., Haralambous, H., and Muslim, B.: Investigation of ionospheric TEC precursors related to the M7.8 Nepal and
M8.3 Chile earthquakes in 2015 based on spectral and statistical analysis, Nat. Hazards, 83, 97–116,
doi:10.1016/10.1007/s11069-016-2409-7, 2016.

Ouzounov, D., Pulinets, S., Davidenko, D., Rozhnoi, A., Solovieva, M., Fedun, V., Dwivedi, B. N., Rybin, A., Kafatos, M.,
660 and Taylor, P.: Transient Effects in Atmosphere and Ionosphere Preceding the 2015 M7.8 and M7.3 Gorkha-Nepal
Earthquakes, Front. Earth Sci., 9, 10.3389/feart.2021.757358, 2021.

Pandey, P. and Rawat, R. S.: Some new observations on the Amritpur Granite Series, Kumaun Lesser Himalaya, India, Curr.
Sci., 77, 296-299, 1999.

Phanikumar, D. V., Maurya, A. K., Kumar, K. N., Venkatesham, K., Singh, R., Sharma, S., and Naja, M.: Anomalous
665 variations of VLF sub-ionospheric signal and Mesospheric Ozone prior to 2015 Gorkha Nepal Earthquake, Sci. Rep., 8, 1-9,
https://doi.org/10.1038/s41598-018-27659-9, 2018.

Pulinets S. A.and Ouzounov D.: Lithosphere–atmosphere–ionosphere coupling (LAIC) model—An unified concept for
earthquake precursors validation, J. Asian Earth Sci., 41, 371–382, https://doi.org/10.1016/j.jseaes.2010.03.005, 2011.

Pulinets, S. A. and Boyarchuk K. A.: Ionospheric Precursors of Earthquakes. Springer, Berlin, Germany, 2004.

670 Pulinets, S. A., Boyarchuk, K. A., Hegai, V. V., Kim, V. P., and Lomonosov, A. M.: Quasielectrostatic model of atmosphere-
thermosphere-ionosphere coupling, Adv. Space Res., 26, 1209-1218, https://doi.org/10.1016/S0273-1177(99)01223-5, 2000.

Pulinets, S. A., Legen'ka A. D. and Alekseev, V. A.: Pre-earthquakes effects and their possible mechanisms, in: Dusty and
Dirty Plasmas, Noise and Chaos in Space and in the Laboratory, edited by: Kikuchi, H., Plenum Publishing, New York, USA,
545-557, https://doi.org/10.1007/978-1-4615-1829-7, 1994.

675 Pulinets, S. A.: Lithosphere-atmosphere-ionosphere coupling (LAIC) model: Electromagnetic Phenomena Associated with
Earthquakes. Transworld Research Network, Trivandrum, India, 2009.

Qi, Y., Wu, L., Ding, Y., Mao, W.: Microwave brightness temperature anomalies associated with the 2015 Mw 7.8 Gorkha
and Mw 7.3 Dolakha earthquakes in Nepal, IEEE Trans. Geosci. Remote Sens., 60, 1-11, doi: 10.1109/TGRS.2020.3036079,
2022

680 Qi, Y., Wu, L., He, M., and Mao, W.: Spatio–temporally weighted twostep method for retrieving seismic MBT anomaly: May
2008 Wenchuan earthquake sequence being a case, IEEE J. Sel. Topics Appl. Earth Observ. Remote Sens., 13, 382-391, doi:
10.1109/JSTARS.2019.2962719, 2020.

Qin, K., Wu, L., De Santis, A., Meng, J., Ma, W., Cianchini, G.: Quasi-synchronous multi-parameter anomalies associated
with the 2010–2011 New Zealand earthquake sequence, Nat. Hazards Earth Sys. Sci., 12, https://doi.org/10.5194/nhess-12-
685 1059-2012, 2012.

Qin, K., Wu, L., Zheng, S., and Liu, S.: A deviation-time-space thermal (DTS-T) method for global Earth observation system of systems (GEOSS)-based earthquake anomaly recognition: Criterions and quantify indices, Remote Sens., 5, 5143-5151, https://doi.org/10.3390/rs5105143, 2013

Qin, K., Zheng, S., Wu, L., and Wang, Y.: Quasi-synchronous multi-parameter anomalies before Wenchuan and Yushu
690   earthquakes in China, The European Phys. J. Spec. Top., 230, 263-274, doi:10.1140/epjst/e2020-000253-3, 2021.

Rycroft, M. J., Harrison, R. J., Nicoll, K. A., and Mareev, E. A.: An overview of Earth's global electric circuit and atmospheric conductivity, Space Sci. Rev., 137, 83-105, https://doi.org/10.1007/s11214-008-9368-6, 2008.

Sapkota, S.N., Bollinger, L., Klinger, Y., Tapponnier, P., Gaudemer D, Y., and Tiwari, D.: Primary surface ruptures of the great Himalayan earthquakes in 1934 and 1255, Nat. Geosci.,6, 71-76, https://doi.org/10.1038/NGEO1669, 2013.

695   Shah, M., and Jin, S. G.: Pre–seismic Thermal Anomalies of the 2015 Mw=7.8 Gorkha (Nepal) Earthquake from MODIS Surface Temperature, in: 2016 Progress in Electromagnetic Research Symposium. IEEE, Shanghai, China, 4755-4758, 2016.

Shalimov, S. L.and Gokhberg, M. B.: Lithosphere–ionosphere coupling mechanism and its application to the earthquake in Iran on June 20, 1990. A review of ionospheric measurements and basic assumptions, Phys. Earth Planet. Inter., 105, 211-218, https://doi.org/10.1016/S0031-9201(97)00092-7, 1998.

700   Shan, X., Zhang, G., Wang, C., Li, Y., Qu, C., Song, X., Yu, L., and Liu, Y.: Joint inversion for the spatial fault slip distribution of the 2015 Nepal MW7.9 earthquake based on InSAR and GPS observations, Chinese J. Geophys. Chinese Edition, 58, 4266-4276, doi: 10.6038/cjg20151131, 2015.

Shen, X. H., Wu, Y. and Shan, X. J.: Remote sensing application in earthquake science and general proposal for earthquake satellite project in China, Recent Dev. World Seismol., 8, 38-45, https://doi.org/10.3969/j.issn.0253-4975.2007.08.011, 2007.

705   Shen, X. H.: Preface to the special issue on satellite application to earthquake science, Acta Seismol. Sin., 38, 3, 329-332, https://doi.org/ 10.11939/jass.2016.03.001, 2016.

Sorokin, V. M. and Chmyrev, V. M.: Modication of the ionosphere by seismic related electric field, Seismo-Electromagnetics. Terra Scientific Publishing Company, Tokyo, Japan, 1998.

Sreejith, K., M., Sunil, P., S., Agrawal, R., Saji, A., P., and Rajawat, A., S.: Coseismic and early postseismic deformation due
710   to the 25 April 2015, Mw 7.8 Gorkha, Nepal, earthquake from InSAR and GPS measurements, Geophys. Res. Lett., https://doi.org/10.1002/2016GL067907, 2016.

St-Laurent, F., Derr, J. S., and Freund, F. T.: Earthquake lights and the stress-activation of positive hole charge carriers in rocks, Phys. Chem. Earth, 31, 305-312, 10.1016/j.pce.2006.02.003, 2006.

Su, X., Wang, Z., Meng, G., Xu, W., and Ren, J.: Pre–seismic strain accumulation and co–seismic deformation of the 2015
715   Nepal MS 8.1 earthquake observed by GPS, Chin. Sci. Bull., 60, 2115-2123, doi: 10.1360/N972015-00534, 2015.

Sun, K., Shan, X., Ouzounov, D, Shen, X., and Jing, F.: Analysing long wave radiation data associated with the 2015 Nepal earthquakes based on Multi–orbit satellite observations, Chinese J. Geophys., 60, 3457-3465, doi: 10.6038/cjg20170915, 2017.

Tang, J., and Yuan, Y. B.: Multi-dimensional distribution of near-field ionospheric disturbances produced by the 2015 Mw7. 8 Nepal earthquake, J. Asian. Earth., 147, 28-36, https://doi.org/10.1016/j.jseaes.2017.07.039, 2017.

720   Teng, J. W.: The exchange of substance and energy, different sphere coupling and deep dynamical process within the earth, Earth Sci. Front., 8, 1-8, https://doi.org/10.3321/j.issn:1005-2321.2001.03.001, 2001.

Tian, Z., Freymueller, J. T., and Yang, Z.: Spatio-temporal variations of afterslip and viscoelastic relaxation following the M-w 7.8 Gorkha (Nepal) earthquake, Earth Planet. Sci. Lett., 531, 10.1016/j.epsl.2019.116031, 2020.

Tronin, A., A.: Thermal IR satellite sensor data application for earthquake research in China, Int. J. Remote Sens., 21, 3169-
725   3177, https://doi.org/10.1080/01431160050145054, 2000.

Ulukavak, M., and Inyurt, S.: Seismo-ionospheric precursors of strong sequential earthquakes in Nepal region, Acta. Astronaut., 166, 123-130, doi: 10.1016/j.actaastro.2019.09.033, 2020.

Wang, K. and Fialko, Y.: Observations and Modeling of Coseismic and Postseismic Deformation Due To the 2015 M-w 7.8 Gorkha (Nepal) Earthquake, J. Geophys. Res. Solid Earth, 123, 761-779, 10.1002/2017JB014620, 2018.

730   Warwick, J. W., Stoker, C., and Meyer, T. R.: Radio emission associated with rock fracture - Possible application to the great Chilean earthquake of May 22, 1960, J. Geophys. Res., 87, 2851-2859, 10.1029/JB087iB04p02851, 1982.

Wu, H.: Multi-parametric analysis of earthquake precursors, Russ. J. Earth. Sci., 15, 1-6, doi: 10.2205/2015ES000553, 2015.

Wu, L. X., Cui, C. Y., Geng, N. G., and Wang, J.H.: Remote sensing rock mechanics (RSRM) and associated experimental studies, Inter. J. Rock Mech. Mining Sci., 37, 879-888, https://doi.org/10.1016/S1365-1609(99)00066-0, 2000

735   Wu, L. X., Liu, S. J., Wu, Y. H., and Wang, C. Y.: Precursors for rock fracturing and failure—Part I: IRR image abnormalities, Int. J. Rock Mech. Mining Sci., 43, 473–482, https://doi.org/10.1016/j.ijrmms.2005.09.002, 2006.

Wu, L. X., Liu, S. J., Wu, Y. H., and Wang, C. Y.: Precursors for rock fracturing and failure—Part II: IRR T-curve abnormalities, Int. J. Rock Mech. Mining Sci., 43, 483–493, https://doi.org/10.1016/j.ijrmms.2005.09.001,2006.

Wu, L. X., Qin, K. and Liu, S. J.: GEOSS-based thermal parameters analysis for earthquake anomaly recognition, Proc. IEEE,
740   100, 2891–2907, https://doi.org/10.1109/JPROC.2012.2184789, 2012.

Wu, L., Qin, K., Liu, S, Santis, and A. D. Cianchini, G.: Importance of lithosphere- coversphere- atmosphere coupling to earthquake anomaly recognition, in: IEEE International Geoscience and Remote Sensing Symposium, Munich, Germany, 2012b.

Wu, L. X., Zheng, S., De Santis, A., Qin, K., Di Mauro, R., Liu, S. J. and Rainone, M. L.: Geosphere coupling and hydrothermal
745   anomalies before the 2009Mw 6.3 L'Aquila earthquake in Italy, Nat. Hazards Earth Syst. Sci., 16, 1859-1880, 2016.

X. Lu, Q. Y. Meng, X. F. Gu, X. D. Zhang, T. Xie, F. Geng, "Thermal infrared anomalies associated with multi–year earthquakes in the Tibet region based on China's FY–2E satellite data," Adv. Space Res., vol. 58, no. 6, pp. 989–1001, 2016.

Xi, J., Ma, A., Guan, H., Chao, L., Nan, Z., Guan, X., Yang, X., Zhang, Z., Zhuoga, C., and Drolma, K.: Analysis and study on the change of the observed geoelectric field data at Lhasa geomagnetic station before and after the Nepal MS8. 1 earthquake,
750   Earthquake Res. China, 30, 2016.

Xiong, P., Tong, L., Zhang, K., Shen, X., Battiston, R., Ouzounov, D., Iuppa, R., Crookes, D., Long, C., and Zhou, H.: Towards advancing the earthquake forecasting by machine learning of satellite data, Sci. Total Enviro. 771, 10.1016/j.scitotenv.2021.145256, 2021.

Yang, X., Sun, L., Sun, C., and Li, L.: Relation between the water temperature anomaly of Yushu well and Nepal Ms8.1
755   earthquake, Plateau Earthq. Res., 28, 12-15, 2016.

Yukutake, Y., Iio, Y., and Horiuchi, S.: Detailed spatial changes in the stress field of the 1984 western Nagano earthquake
region, J. Geophys. Res. Solid Earth, 115, 10.1029/2008JB006111, 2010.

Zhan, W., Wu, Y., Liang, H., Zhu, S., Zhang, F., and Liu, J.: Characteristics of the seismogenic model for the 2015 Nepal
M_w7.8 earthquake derived from GPS data, Chinese J. Geophys., 58, 1818-1826, doi: 10.6038/cjg20150532, 2015.

760   Zhang, X., Zhang, Y., Guo, X., Wei, C., and Zhang, L.: Analysis of thermal infrared anomaly in the Nepal Ms 8.1 earthquake,
Earth Sci. Frontiers, 24, 227-233, 2017.

Zhao, B., Buergmann, R., Wang, D., Tan, K., Du, R., and Zhang, R.: Dominant Controls of Downdip Afterslip and Viscous
Relaxation on the Postseismic Displacements Following the M(w)7.9 Gorkha, Nepal, Earthquake, J. Geophys. Res. Solid Earth,
122, 8376-8401, 10.1002/2017JB014366, 2017.

765   Zheng, G., Wang, H., Wright, T. J., Lou, Y. D., Zhang, R., Zhang, W. X., Shi, C., Huang, J. F.,and Wei, N.: Crustal deformation
in the India-Eurasia collision zone from 25 years of GPS measurements, J. Geophys. Res. Solid Earth., 122, 9290–9312,
https://doi.org/10.1002/2017JB014465, 2017.

Zheng, S., Wu, L. X., and Qin, K.: Multiple parameters anomalies for verifying the geosystem spheres coupling effect: a case
study of the 2010 Ms7.1 Yushu earthquake in China, Ann. Geophy., 57, 10.4401/ag-6508, 2014.

770   Zhou, Z. L., Chang, Y., and Cai, X.: Experimental study of infrared radiation effects of rock with different loading rates, J.
Central South Univ. (Sci. and Tech.)., 50, 1127-1134, https://doi.org/10.11817/j.issn.1672-7207.2019.05.016, 2019.